NASA TECHNICAL NOTE

NASA TN D-5885

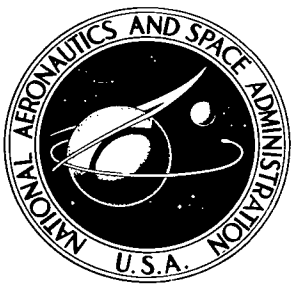

AERODYNAMIC CHARACTERISTICS OF A HYPERSONIC TRANSPORT CONFIGURATION AT MACH 6.86

by William J. Small, Frank S. Kirkham, and David E. Fetterman

Langley Research Center
Hampton, Va. 23365

NATIONAL AERONAUTICS AND SPACE ADMINISTRATION • WASHINGTON, D. C. • JUNE 1970

1. Report No.	2. Government Accession No.	3. Recipient's Catalog No.
NASA TN D-5885		

4. Title and Subtitle
AERODYNAMIC CHARACTERISTICS OF A HYPERSONIC TRANSPORT CONFIGURATION AT MACH 6.86

5. Report Date
June 1970

6. Performing Organization Code

7. Author(s)
William J. Small, Frank S. Kirkham, and David E. Fetterman

8. Performing Organization Report No.
L-6803

9. Performing Organization Name and Address
NASA Langley Research Center
Hampton, Va. 23365

10. Work Unit No.
722-01-10-09

11. Contract or Grant No.

12. Sponsoring Agency Name and Address
National Aeronautics and Space Administration
Washington, D.C. 20546

13. Type of Report and Period Covered
Technical Note

14. Sponsoring Agency Code

15. Supplementary Notes

16. Abstract

An investigation of a model representative of a hypersonic transport has been conducted at a Mach number of 6.86 over a range of Reynolds numbers, based on body length, of 1×10^6 to 6×10^6. The configuration was a low-wing, distinct wing-body arrangement with a body-mounted vertical tail and an underwing propulsion system. The complete vehicle and the contribution of its components are analyzed in order to evaluate the performance of this class of vehicle. Present methods of predicting aerodynamic performance were also evaluated.

17. Key Words (Suggested by Author(s))
Hypersonic transport
Interference
Stability

18. Distribution Statement
Unclassified – Unlimited

19. Security Classif. (of this report)	20. Security Classif. (of this page)	21. No. of Pages	22. Price*
Unclassified	Unclassified	24	$3.00

*For sale by the Clearinghouse for Federal Scientific and Technical Information
Springfield, Virginia 22151

AERODYNAMIC CHARACTERISTICS OF A HYPERSONIC TRANSPORT CONFIGURATION AT MACH 6.86

By William J. Small, Frank S. Kirkham,
and David E. Fetterman
Langley Research Center

SUMMARY

An investigation of a model representative of a hypersonic transport has been conducted at a Mach number of 6.86 over a range of Reynolds numbers, based on body length, of 1×10^6 to 6×10^6. The configuration was a low-wing, distinct wing-body arrangement with a body-mounted vertical tail and an underwing propulsion system. The complete vehicle and the contribution of its components are analyzed in order to evaluate the performance of this class of vehicle.

The configuration studied exhibited relatively low maximum lift-drag characteristics (near 3) under tunnel conditions. This poor performance was caused by the large-volume-body design and by adverse interference effects caused by this fuselage and its associated boundary-layer diverter. Present methods of predicting aerodynamic performance were evaluated and found to be inadequate.

INTRODUCTION

Trade-off studies (refs. 1, 2, and 3) have obtained preliminary optimization of hypersonic transport vehicles by exercising system variables, some of which are vehicle weight, cruise Mach number, wing loading, power-plant sizing, and body fineness ratio. The studies examined hydrogen-fueled, turboramjet-powered aircraft at cruise Mach numbers of about 6. Because of the low density of the liquid-hydrogen fuel considered for these aircraft, trade-offs between structural and aerodynamic areas indicate that hypersonic transport configurations will optimize with a low-fineness-ratio body, having a large volume in relation to the wing area. Inputs to these system studies have been largely analytical with little experimental verification. Additional studies are now required to verify or improve these techniques and to enable more realistic inputs to future trade-off studies.

The theoretical and experimental investigation reported herein was undertaken to obtain hypersonic aerodynamic characteristics of a typical, distinct wing-body, hypersonic transport configuration and to provide a better knowledge of the contributions provided by

the various vehicle components. The study focused on a distinct delta-wing—body arrangement with body-mounted vertical tail, low-wing position, and engine nacelle located beneath the wing. For this arrangement, most of the local configuration problem areas encountered on a complete vehicle design are represented. The model was proportioned according to the results of reference 2 and tested at a Mach number of 6.86. The resulting analysis, presented in this paper, was carried out with the intent of assessing the limitations of current theoretical techniques and of determining the general aerodynamic efficiencies of the major vehicle components and their relative contribution to the total lift and drag.

SYMBOLS

C_D drag coefficient, $\frac{\text{Drag}}{qS_w}$

$C_{D,o}$ drag coefficient at $\alpha = 0^o$

$C_{D_{p,o}}$ pressure-drag coefficient at $\alpha = 0^o$

$\frac{dC_D}{dC_L^2}$ drag-due-to-lift parameter (This parameter is evaluated at its average value between 8^o and 12^o angle of attack)

C_L lift coefficient, $\frac{\text{Lift}}{qS_w}$

C_l rolling-moment coefficient, $\frac{\text{Rolling moment}}{qS_w\bar{c}}$

C_{l_β} effective-dihedral parameter, $\frac{\partial C_l}{\partial \beta}$, per deg

C_m pitching-moment coefficient, $\frac{\text{Pitching moment}}{qS_w\bar{c}}$

C_N normal-force coefficient, $\frac{\text{Normal force}}{qS_w\bar{c}}$

C_n yawing-moment coefficient, $\frac{\text{Yawing moment}}{qS_w\bar{c}}$

C_{n_β} directional-stability parameter, $\frac{\partial C_n}{\partial \beta}$, per deg

C_p pressure coefficient

C_Y	side-force coefficient, $\frac{\text{Side force}}{qS_w}$
C_{Y_β}	side-force parameter, $\frac{\partial C_Y}{\partial \beta}$, per deg
c	chord
$\bar{c}$	mean aerodynamic chord of complete delta wing
$\frac{L}{D}$	lift-drag ratio
l	body length
M	free-stream Mach number
q	free-stream dynamic pressure
R_l	Reynolds number based on body length
r	radius
S_P	planform area
S_w	wing area
T	temperature
V	total volume
$\frac{V^{2/3}}{S_P}$	volume parameter
$\frac{x_{ac}}{\bar{c}}$	static margin, $\frac{dC_m}{dC_N}$
α	angle of attack, deg
β	angle of sideslip, deg
δ_e	elevon deflection angle, deg (negative when trailing edge is up)

Subscripts:

t	stagnation conditions
W	wall conditions
max	maximum
trim	trimmed condition

MODEL

A drawing of the model is shown in figure 1. The model is intended to represent a 300-foot- (91.44-meter-) long hypersonic transport with a gross take-off weight of 500 000 lbf (2224 kN), which is designed to cruise in a Mach number range from 6 to 8. The body volume is sized to contain the payload and the hydrogen fuel required for a 5000-nautical-mile (9260-km) mission. The vehicle wing loading is 70 lbf/ft^2 (3.35 kN/m^2). The overall volume parameter $V^{2/3}/S_P$, including the wing volume, is 0.22.

The fineness-ratio-14 body has a negatively cambered forebody to improve the trim characteristics of the aircraft. The forebody cross sections are circular forward of the wing apex. Aft of the wing apex, these circular cross sections are gradually transformed into flat-sided cross sections with semicircular tops to provide a nearly perpendicular juncture between the wing and body.

The 75°-sweep, flat-bottomed delta wing is set at a 3.15° incidence to the body. The wing is 2.8-percent thick with maximum thickness at 2/3 chord and with sharp leading and trailing edges. A boundary-layer diverter is located in the region of the wing apex and is approximated on the model by a 15° half-angle wedge-shaped fillet. The elevons extend the entire span of the wing outboard of the engine nacelle and have an area equal to 14 percent of the wing planform area.

The vertical tail has a 70°-sweep leading edge with a semiwedge angle of 4°. The trailing edge is blunt and swept 30°. The tail planform area is 14 percent of the wing planform area.

The engine nacelle is located beneath the wing and behind the wing-leading-edge shocks to take advantage of the precompressed flow beneath the wing. The ratio of inlet width to height is 4, and the inlet capture area was 1.4 percent of the wing planform area. The inlet side plates are swept 76.05° and have a 4.98° external wedge angle along the sharp leading edges. The nacelle has a constant internal duct area and an overall

external exit-to-inlet-area ratio of 1.07 because of the finite thickness of the nacelle walls. The rear of the nacelle was coincident with the wing trailing edge.

By removing the wing from the wing-body model along the separation line shown in figure 1, the model could be tested as a body-alone configuration. The vertical tail could be removed at the vertical-tail—body juncture for those tests of the model without a vertical tail.

APPARATUS AND TESTS

Tests were conducted in the Langley 11-inch hypersonic tunnel at a Mach number of 6.86, at Reynolds numbers, based on the body length, from 1×10^6 to 6×10^6. Tunnel stagnation temperature was in excess of 1060° R (589° K) for all tests, and water-condensation effects were prevented by keeping the absolute humidity of the air less than 1.9×10^{-5} parts of water per part of dry air by weight. Further details of the characteristics of this wind tunnel can be found in reference 4.

Forces and moments on the model were measured with a six-component strain-gage internal balance. Body base pressure was measured at two positions, one position near the upper part of the base and the other on the lower part. These two pressures were averaged to give the effective average base pressure. The vehicle axial force was then corrected to a value equivalent to that for free-stream static pressure on the base. All data were corrected for nacelle internal drag (estimated skin friction) and for nacelle base drag. The nacelle base pressure was not measured but was calculated by the following equation:

$$C_p = -\frac{1}{M^2}$$

ACCURACY OF DATA

The errors resulting from the force-balance inaccuracies, uncertainties in angle of attack, and base pressures are estimated to be as follows:

Configuration	R_l	Error, percent, in –			
		C_m	C_L	C_D	L/D
Body alone	1×10^6	9.2	15.2	11.0	39.7
	6	1.3	2.4	3.1	13.7
Wing-body-tail-nacelle	1×10^6	0.1	4.8	4.5	17.8
	6	.02	.8	1.4	5.4

RESULTS AND DISCUSSION

Comparisons of Theoretical Results With Experimental Data

Studies of hypersonic cruise vehicles rely on analytic prediction techniques to provide aerodynamic inputs to system trade-off studies and to help define aerodynamically attractive configuration concepts. It is of interest, therefore, to examine the validity of predictions provided by present hypersonic analytic methods which treat the configuration as a combination of isolated components with the forces on each component being calculated as if the component were isolated in the free-stream flow.

The configuration investigated was analyzed theoretically by dividing it into major components, the body, wing, tail, nacelle, leading edges, and wing-body fillet. A comparison of theory with experiment was made at a Reynolds number R_l of 1×10^6, where the boundary layer is expected to be predominately laminar. (Results from ref. 5 show that the beginning of transition in the same wind tunnel occurs approximately at a Reynolds number of 1.3×10^6 on a sharp flat plate. Refs. 6 and 7 indicate, however, that transition may occur much sooner in wing-body-juncture regions and on highly swept delta wings.) Theoretical calculations of the laminar skin friction were made by the reference-temperature method (ref. 8) by assuming all vehicle surfaces as combinations of tapered flat plates and cones and for a T_W/T_t of 0.5. Skin friction was calculated for the zero-angle-of-attack condition only and was assumed to be constant throughout the angle-of-attack range.

Of the various theoretical methods presented in figure 2(a) for the body alone, results from Newtonian theory $\left(C_{p,max} = 2.0 \text{ and } C_p = 0 \text{ in shadow region}\right)$ agreed best with the experimental data; thus this theory was selected for the remaining calculations. Although this agreement is consistent with the results of references 9 and 10, it is inconsistent with the results of reference 11 and with recent unpublished data obtained on the fuselage of the delta-wing—body configuration of reference 3, for which the tangent-cone and Prandtl-Meyer expansion theories gave good predictions of experimental results. It appears that reliable a priori results will be obtained only after a more rigorous theoretical method is developed.

The aerodynamic pressure forces on wing and tail surfaces were calculated by shock-expansion theory, which has been shown to give good results for delta wings at low angles of attack. (See ref. 12.) The aerodynamic pressure forces on the nacelle external wedge angles were calculated by using tangent-wedge flow and the assumption that the nacelle was located within a uniform lower wing surface flow. Newtonian theory was used to predict pressure forces on all wing, nacelle, and tail leading edges. Figure 2(b) presents a comparison of theoretical estimates of configuration aerodynamics with experimental results. Since the theories selected should adequately predict the lift forces of the isolated components of the configuration, they should also predict the

overall-configuration lift if no interference forces exist. This, however, is not the case, and the discrepancies between theoretical and experimental lift-coefficient results for the wing-body (also with tail and nacelle additions) configuration must be due to wing-body interference, which includes the adverse effects of the wing-body fillet on the wing upper surface flow field. These effects will be discussed in subsequent sections of this paper. The underprediction of the drag data is believed to be due to a combination of the inadequacy of the theory used to predict the fuselage drag and the previously mentioned interference effects.

The $(L/D)_{max}$ (fig. 2(b)) developed by the configuration is lower than had been considered in studies for similarly sized hypersonic transport aircraft. (See refs. 1 and 2.) Part of the reason for this low $(L/D)_{max}$ (near 3) is the large skin friction encountered under wind-tunnel conditions, the poor aerodynamic efficiencies of the configuration components, and the component interferences. To study these component efficiencies and define possible configuration faults, the drag at $\alpha = 0^{o}$ $\left(C_{D,o}\right)$ and the drag-due-to-lift parameter $dC_D/dC_L{}^2$ are examined.

Drag at $\alpha = 0^{o}$

A breakdown of $C_{D,o}$ is given in figure 3. As indicated, the boundary layer is expected to be predominately laminar at a Reynolds number, based on body length, of 1×10^6. (See fig. 3(a).) The skin-friction drag is estimated to contribute about 60 percent of the total zero angle-of-attack drag. In flight, even though the boundary layer would be predominately turbulent, the skin-friction contribution at the high flight Reynolds number $\left(R_l > 100 \times 10^6\right)$ would be approximately 40 percent of $C_{D,o}$. The experimental results of the component-drag breakdown tests are also shown in figure 3(a). The body-alone tests indicate that the body produces about 40 percent of the drag of the wing-body-tail configuration. The wing, which is charged with the drag of the wing-body fillet and with the drag produced by the mutual interference between the wing and body, is responsible for about 50 percent of $C_{D,o}$. Note that the wing at 3.15^{o} incidence to the vehicle center line develops substantial drag due to lift and thus the wing $C_{D,o}$ is not representative of the wing zero-lift drag.

To further define the component drag contributions, the theoretical contribution of each component to the zero-angle-of-attack pressure drag $C_{D_{p,o}}$ is shown in figure 3(b). The body produces about 20 percent of the pressure drag. A 10-percent reduction in body pressure drag will result in a 7-percent rise in $(L/D)_{max}$ for this configuration. It may be possible to reduce body drag by reducing the body volume through more efficient utilization of available space. Wasted space between fuel tanks, in corners, and so forth, increases total body volume to twice that required to contain fuel and payload. Geometric modifications to the fuselage forebody and more careful attention to afterbody closure contours could also contribute to drag reductions. Careful attention must also be given to

wing-body-juncture design. The negatively cambered body was joined to the flat-bottomed wing in this region by a boundary-layer diverter (a 15° half-angle—wedge fillet), which is estimated to produce 34 percent of $C_{D_{p,o}}$. Redesign or elimination of this wing-body fillet would result in a major reduction in $C_{D_{p,o}}$.

Drag Due to Lift

The drag-due-to-lift parameter dC_D/dC_L^2 is shown as a bar graph in figure 4. The data shown for the exposed wing of the configuration were obtained by subtracting the body-alone data from the wing-body data. (See fig. 4(a).) Thus, the wing is charged with any penalties due to the wing-body juncture and with all the mutual interference effects of the body on the wing and of the wing on the body. Tests were also conducted on the isolated wing (including the wing-body fillet) with a 5° half-cone mounted on the upper surface to contain the force balance. These data are shown by the bar graph labeled "wing-cone fillet." The presence of the cone on the upper surface of the wing would be expected to adversely affect the drag-due-to-lift parameter of the wing. However, the exposed-wing drag due to lift is higher than that of the wing-cone fillet, which indicates that the large-volume body mounted above the wing has a significantly adverse effect on lifting efficiency. Although the difference in the drag-due-to-lift parameter is the total result of the mutual interference effects between the body and wing, the primary reason for this difference is believed to be due to the presence of the body which produces an increased pressure on the fillet and on the wing leeward surface. Redesign or elimination of the wing-body fillet was previously shown to reduce $C_{D_{p,o}}$ and it would also be expected to improve the configuration efficiency through a reduction in dC_D/dC_L^2. The theoretical drag due to lift for a zero-thickness flat-plate wing, which represents the minimum drag due to lift obtainable from a noncambered wing surface, is shown for comparison in figure 4.

Shown in figure 4(b) is a comparison of the lifting efficiency of the configuration body and experimental values for half-cone—cylinder bodies (ref. 13), all of which had equal values of $V^{2/3}/S_P$ and essentially the same included nose angle. The configuration body is as inefficient as the flat-top body, which suggests that a possible improvement in body design would be to incorporate a more flat-bottomed arrangement for that part of the fuselage not shielded by the wing.

A 10-percent reduction in dC_D/dC_L^2 for both the wing and body would improve the overall $(L/D)_{max}$ by about 7 percent.

Trim Characteristics

From weight and balance considerations, the center of gravity was determined to be $0.256\bar{c}$; and, based on the method of reference 14, this center-of-gravity position gives a landing-speed static margin of 0.092.

The longitudinal trim characteristics for this center-of-gravity position are given in figure 5 for the highest test Reynolds number of 6×10^6, where any separation effects should be minimized. The configuration is stable at all attitudes investigated, and only moderate elevon deflection angles are required to trim the aircraft. Addition of the nacelle reduces trimmed $(L/D)_{max}$ by about 7 percent, partly because of the increase in drag associated with the inlet and partly because of the considerably larger elevon deflections required to offset the nose-down pitching moment induced by the nacelle. The static margin of the configuration is slightly increased when the nacelle is added.

Lateral and Directional Stability

The lateral-stability parameters C_{n_β}, C_{l_β}, and C_{Y_β} are shown as a function of angle of attack in figure 6. At $\alpha = 0^o$, the wing-body (also with tail and nacelle additions) configuration is directionally stable (positive C_{n_β}); however, at $\alpha = 6.85^o$, which is close to $(L/D)_{max}$ (see fig. 5), the vertical tail becomes ineffective and the configuration is unstable. This loss in tail effectiveness at an angle of attack is typical of hypersonic configurations of this type and is due to the reduction in local dynamic pressure in the region of the tail brought about by the interference and shielding effects of the body and wing. Reducing the lateral surface area of the forebody by decreasing the height-to-width ratio would be expected to improve the directional stability. The beneficial effects of the nacelle on C_{n_β} increase with α because the nacelle is mounted in the high-pressure field beneath the wing and is thus a more effective stabilizing surface when the wing is at an angle of attack.

All the wing-body configurations exhibited positive effective dihedral (negative C_{l_β}) at all conditions tested.

Basic Data

The basic data from which the foregoing results were obtained are presented in figures 7 to 9.

CONCLUDING REMARKS

An investigation of a model representative of a hypersonic transport has been conducted at a Mach number of 6.86 over a range of Reynolds numbers, based on body length, of 1×10^6 to 6×10^6. The configuration was a low-wing, distinct wing-body arrangement with a body-mounted vertical tail and an underwing propulsion system.

The configuration exhibited relatively low maximum lift-drag characteristics under tunnel conditions. One cause of this poor performance was due to the large-volume-body design, which produced high minimum drag, high drag due to lift, and adverse interference

effects, which reduced the vehicle lifting capability. A large drag increment also resulted from the boundary-layer diverter (wing-body fillet). Improved performance could be obtained through more efficient aerodynamic shaping of the body and elimination of the boundary-layer diverter. Present analytic techniques are, in general, inadequate for predicting the aerodynamic characteristics of these complex vehicles on which component interference effects are important. More research to define these effects more accurately and to develop improved analytic techniques is required.

Langley Research Center,
National Aeronautics and Space Administration,
Hampton, Va., May 6, 1970.

REFERENCES

1. Drake, Hubert M.; Gregory, Thomas J.; and Petersen, Richard H.: Hypersonic Technology Problems Identified in Mission Studies. Conference on Hypersonic Aircraft Technology, NASA SP-148, 1967, pp. 1-19.

2. Gregory, Thomas J.; Petersen, Richard H.; and Wyss, John A.: Performance Tradeoffs and Research Problems for Hypersonic Transports. J. Aircraft, vol. 2, no. 4, July-Aug. 1965, pp. 266-271.

3. Penland, Jim A.; Edwards, Clyde L. W.; Witcofski, Robert D.; and Marcum, Don C., Jr.: Comparative Aerodynamic Study of Two Hypersonic Cruise Aircraft Configurations Derived From Trade-off Studies. NASA TM X-1436, 1967.

4. McLellan, Charles H.; Williams, Thomas W.; and Beckwith, Ivan E.: Investigation of the Flow Through a Single-Stage Two-Dimensional Nozzle in the Langley 11-Inch Hypersonic Tunnel. NACA TN 2223, 1950.

5. Neal, Luther, Jr.: A Study of the Pressure, Heat Transfer, and Skin Friction on Sharp and Blunt Flat Plates at Mach 6.8. NASA TN D-3312, 1966.

6. Dunavant, James C.: Heat Transfer to a Delta-Wing—Half-Cone Combination at Mach Numbers of 7 and 10. NASA TN D-2199, 1964.

7. Deem, Ralph E.; and Murphy, James S.: Flat Plate Boundary Layer Transition at Hypersonic Speeds. AIAA Pap. No. 65-128, Jan. 1965.

8. Monaghan, R. J.: An Approximate Solution of the Compressible Laminar Boundary Layer on a Flat Plate. R. & M. No. 2760, Brit. A.R.C., 1953.

9. Penland, Jim A.; and Fetterman, David E., Jr.: The Effects at a Mach Number of 6.86 of Drag Brakes on the Lift, Drag, and Pitching Moment of an Ogive Cylinder. NACA RM L55K23, 1955.

10. Penland, Jim A.: A Study of the Stability and Location of the Center of Pressure on Sharp, Right Circular Cones at Hypersonic Speeds. NASA TN D-2283, 1964.

11. Goldberg, Theodore, J.; Hefner, Jerry N.; and Stone, David R.: Hypersonic Aerodynamic Characteristics of Two Delta-Wing X-15 Airplane Configurations. NASA TN D-5498, 1969.

12. Fetterman, David E.: A Method for Predicting the Normal-Force Characteristics of Delta Wings at Angles of Attack From 0° to 90°. NASA TM X-757, 1963.

13. Fetterman, David E.: Favorable Interference Effects on Maximum Lift-Drag Ratios of Half-Cone Delta-Wing Configurations at Mach 6.86. NASA TN D-2942, 1965.

14. Anon.: USAF Stability and Control Datcom. Contracts AF 33(616)-6460 and AF 33(615)-1605, Douglas Aircraft Co., Inc., Oct. 1960. (Revised Nov. 1965.)

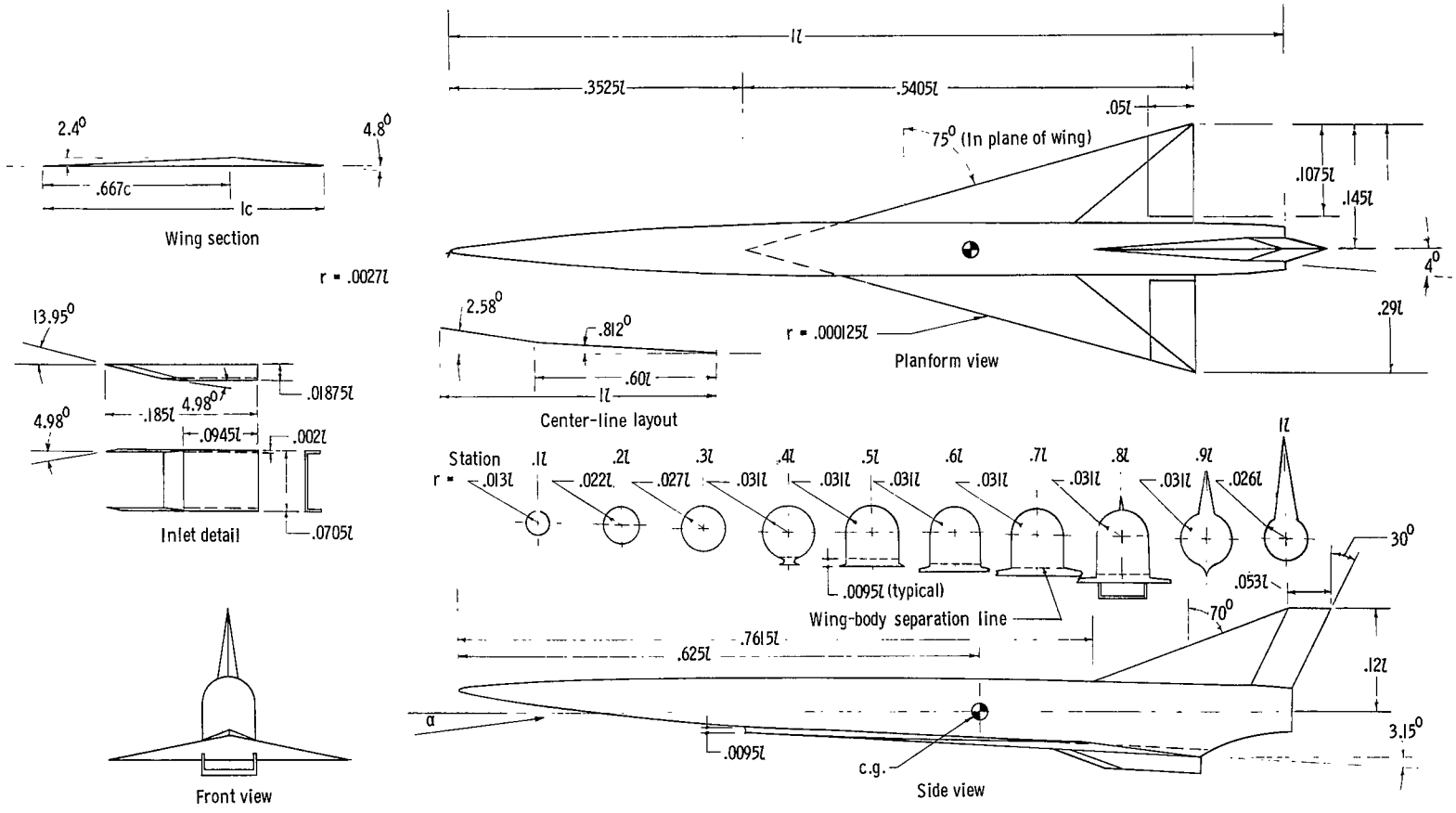

Figure 1.- Configuration detail. All linear dimensions are given in terms of l, where l = 20 inches (50.8 cm).

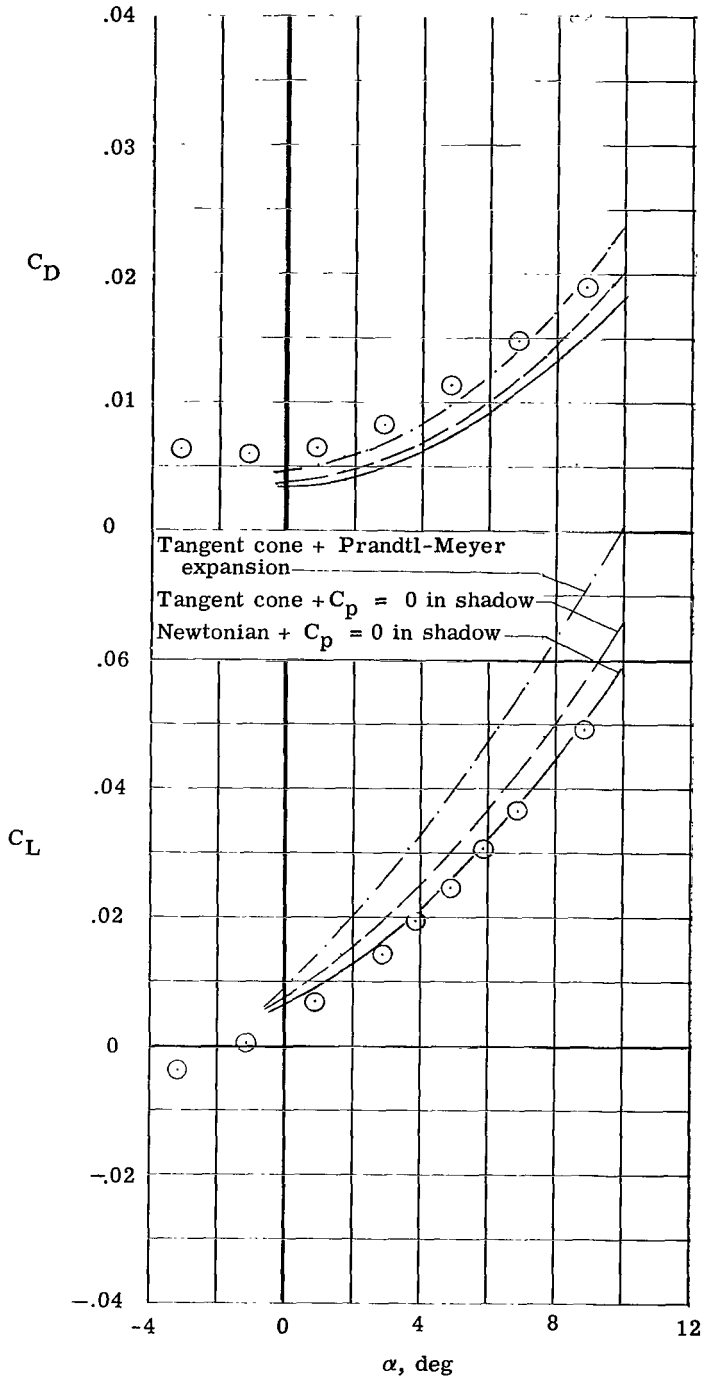

(a) Data for body-alone configuration compared with results from several theories.

Figure 2.- Comparison of theoretical and experimental aerodynamic characteristics. $R_\ell = 1 \times 10^6$.

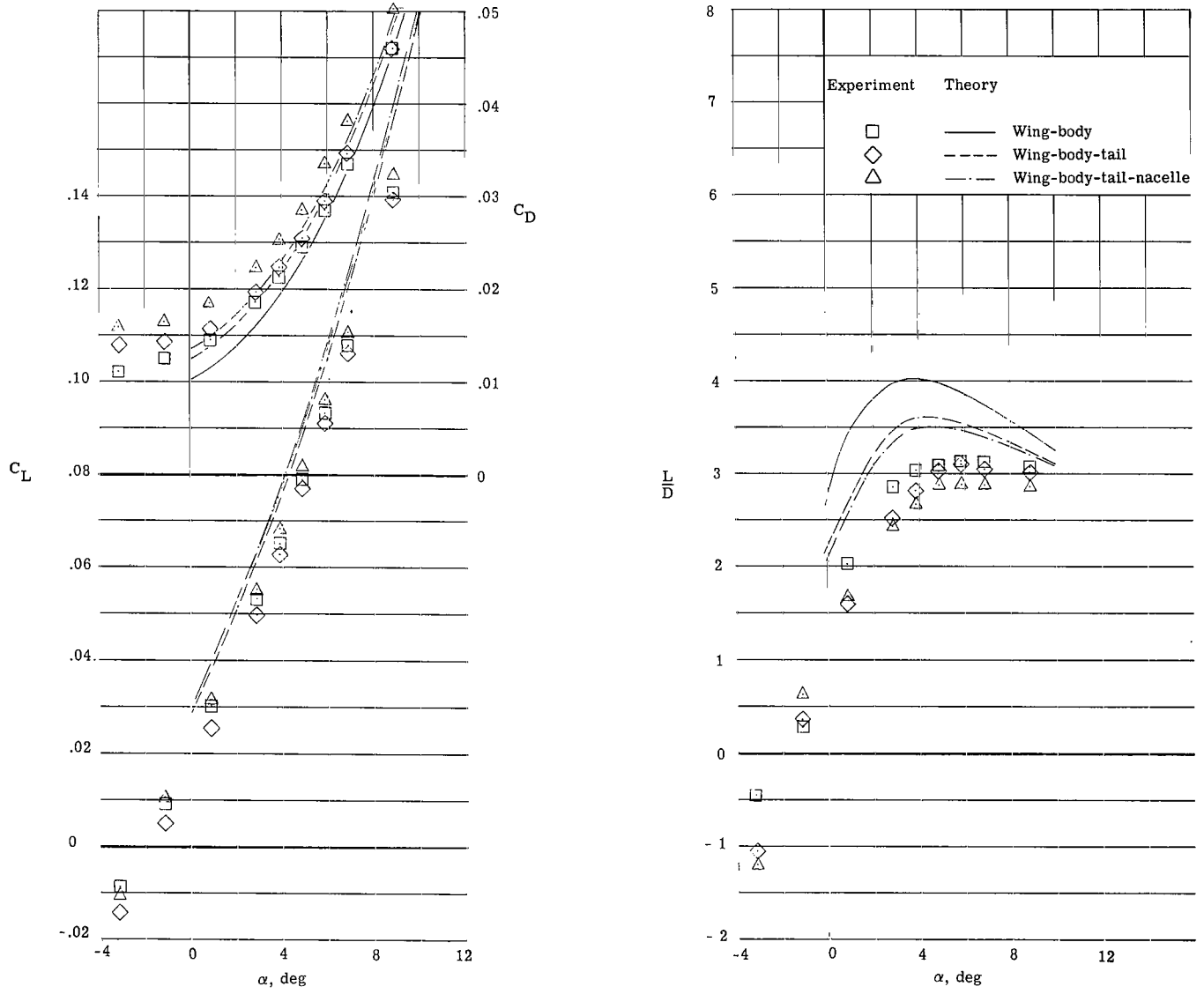

(b) Data for several body configurations compared with results from Newtonian theory ($C_{p,max}$ = 2.0 and C_p = 0 in shadow).

Figure 2.- Concluded.

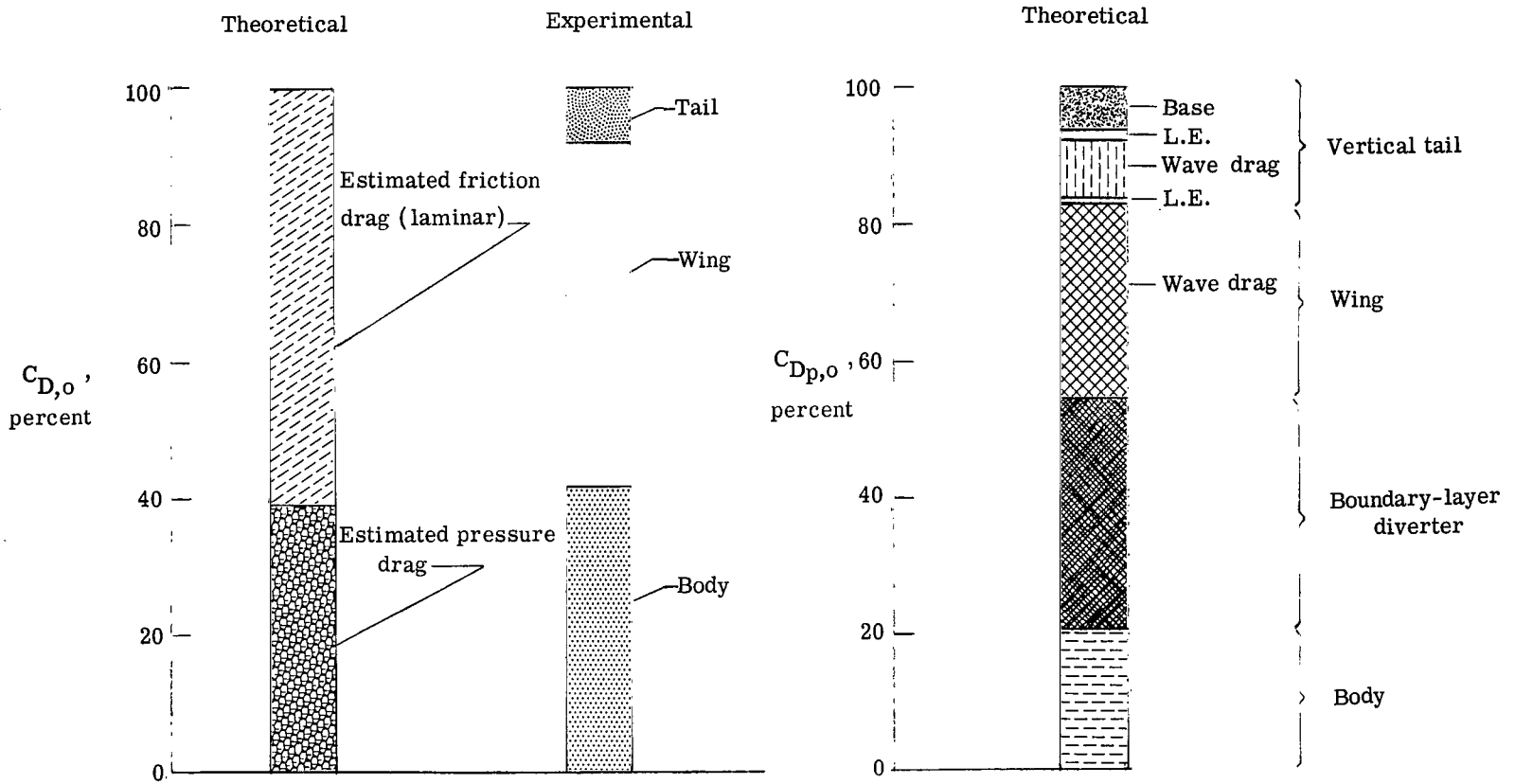

(a) Total drag.

(b) Pressure drag.

Figure 3.- Drag analysis for wing-body-tail configuration. $\alpha = 0^0$; $R_l = 1 \times 10^6$.

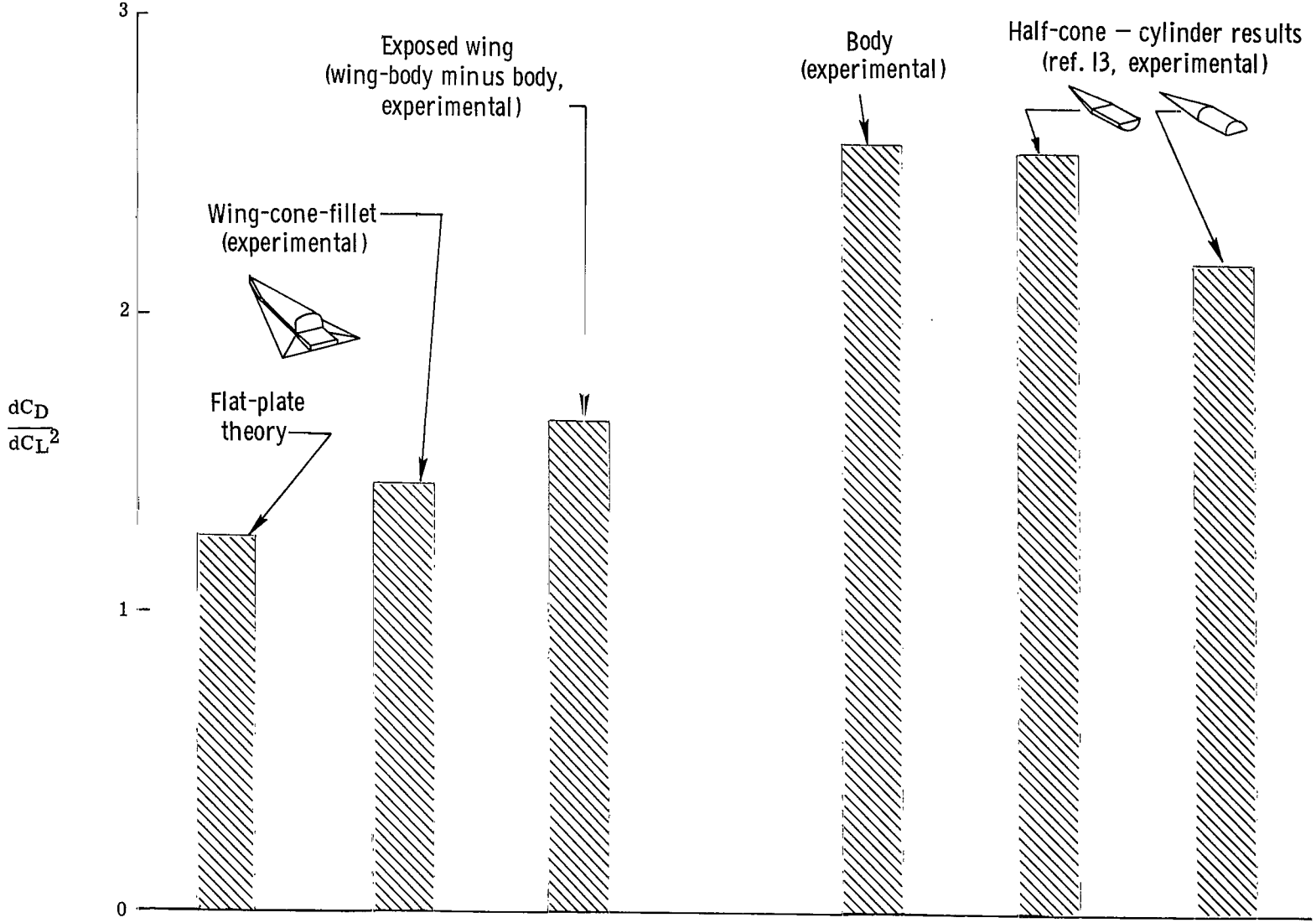

(a) Wing.

(b) Body. $\frac{V^{2/3}}{S_P} = 0.27$.

Figure 4.- Drag due to lift. $R_l = 1 \times 10^6$.

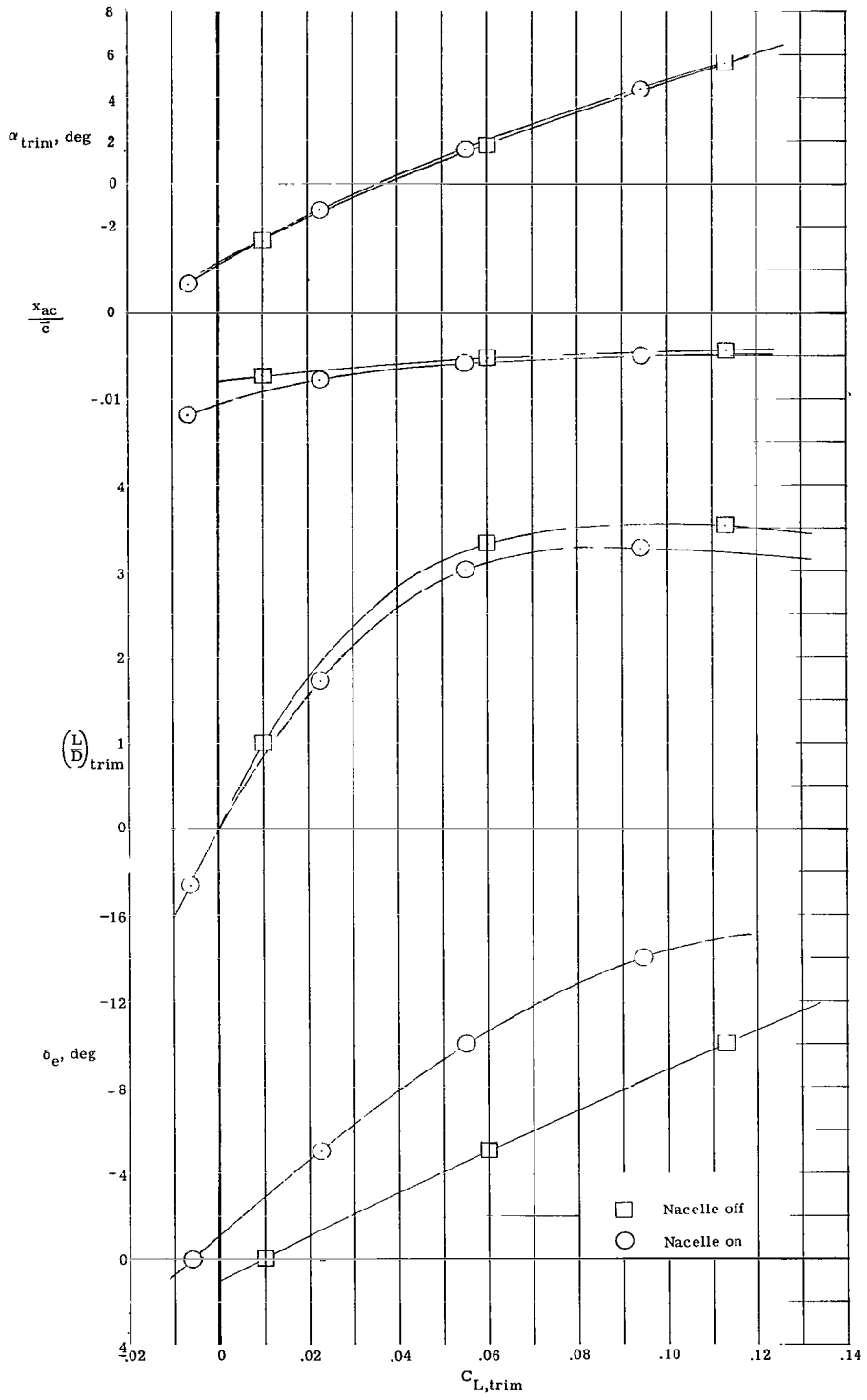

Figure 5.- Longitudinal trim characteristics. $R_l = 6 \times 10^6$.

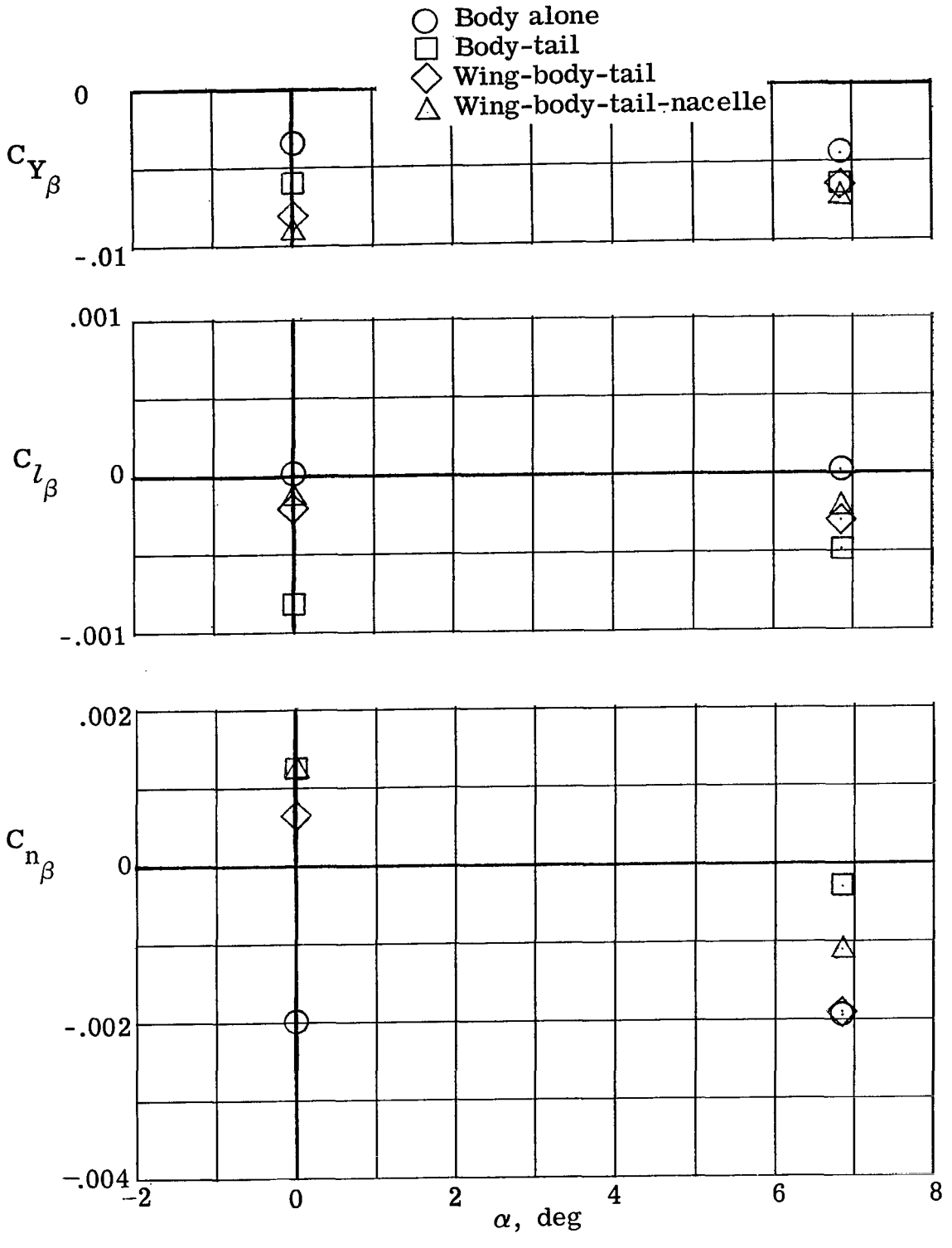

Figure 6.- Lateral aerodynamic characteristics. $R_l = 6 \times 10^6$.

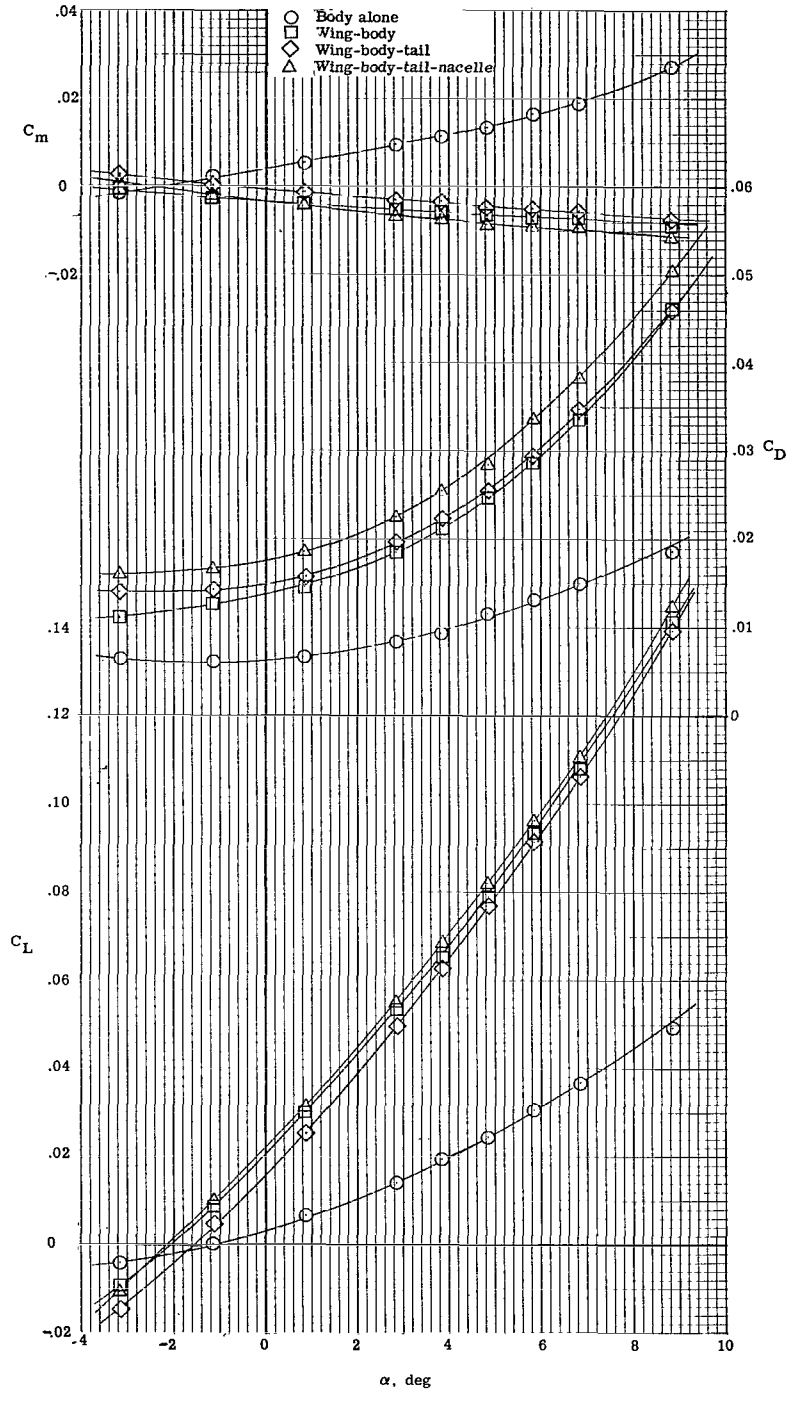

(a) $R_\ell = 1 \times 10^6$.

Figure 7.- Longitudinal aerodynamic characteristics – component breakdown.

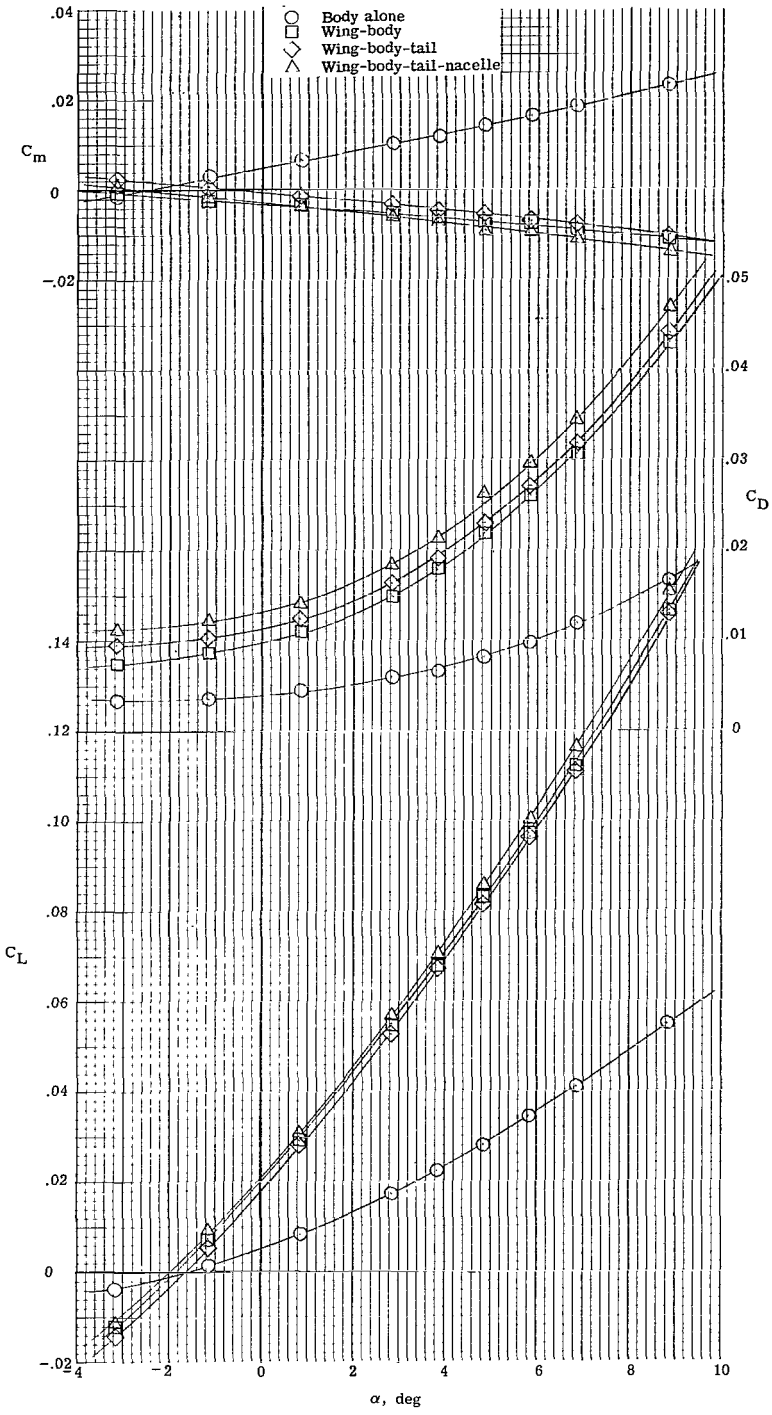

(b) $R_l = 6 \times 10^6$.

Figure 7.- Concluded.

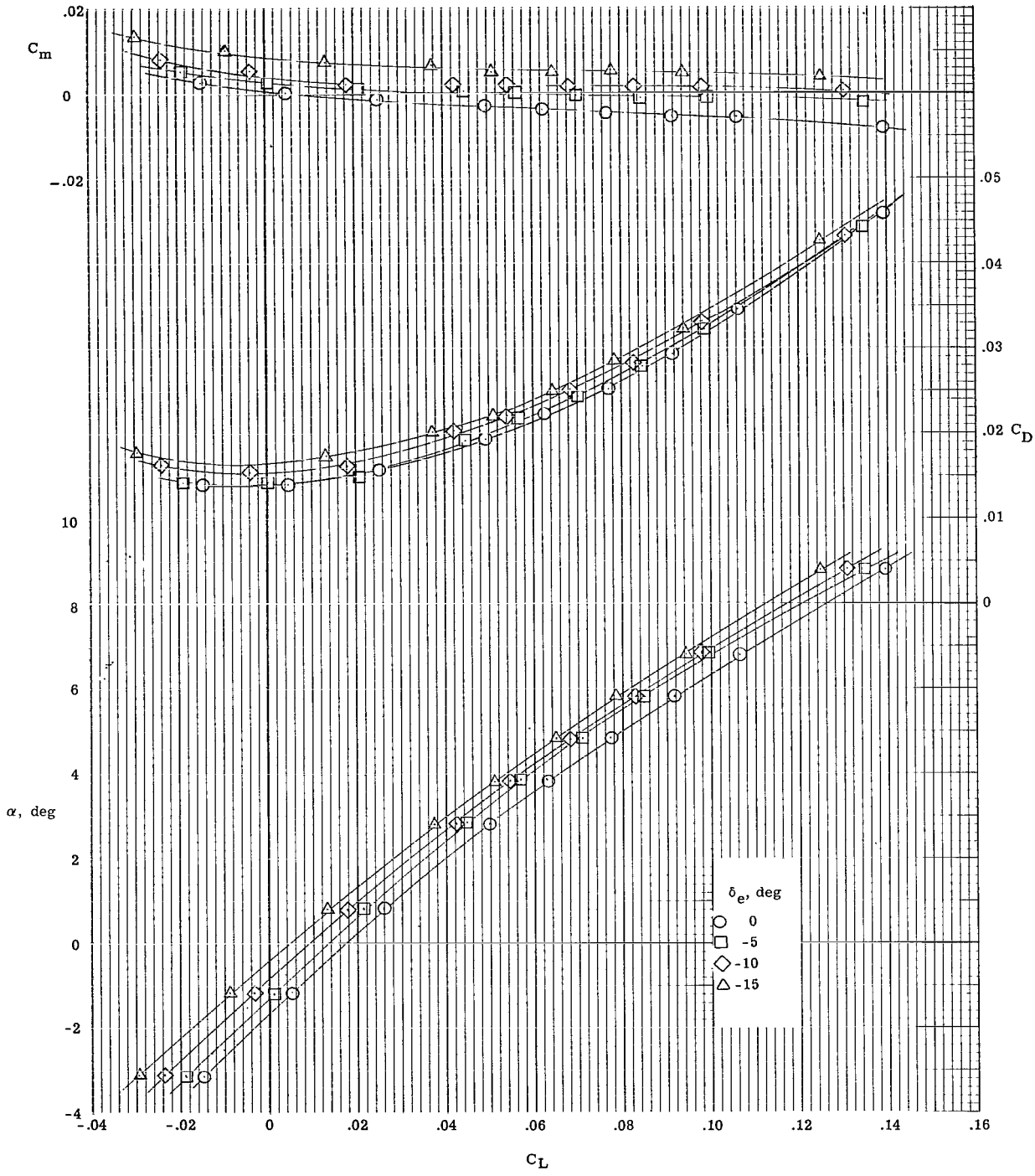

(a) Wing-body-tail. $R_\ell = 1 \times 10^6$.

Figure 8.- Effect of elevon deflection on longitudinal aerodynamic characteristics.

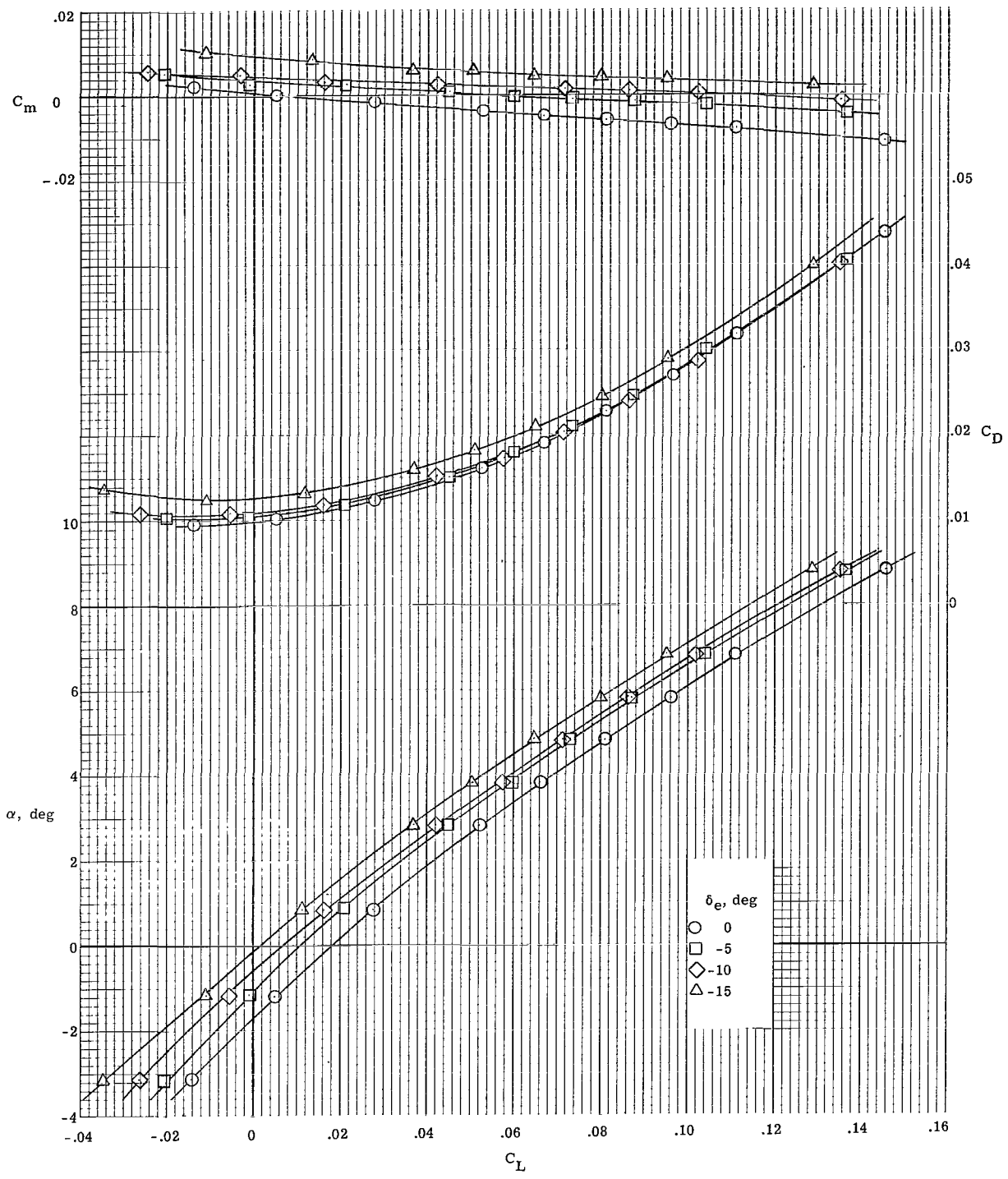

(b) Wing-body-tail. $R_\ell = 6 \times 10^6$.

Figure 8.- Continued.

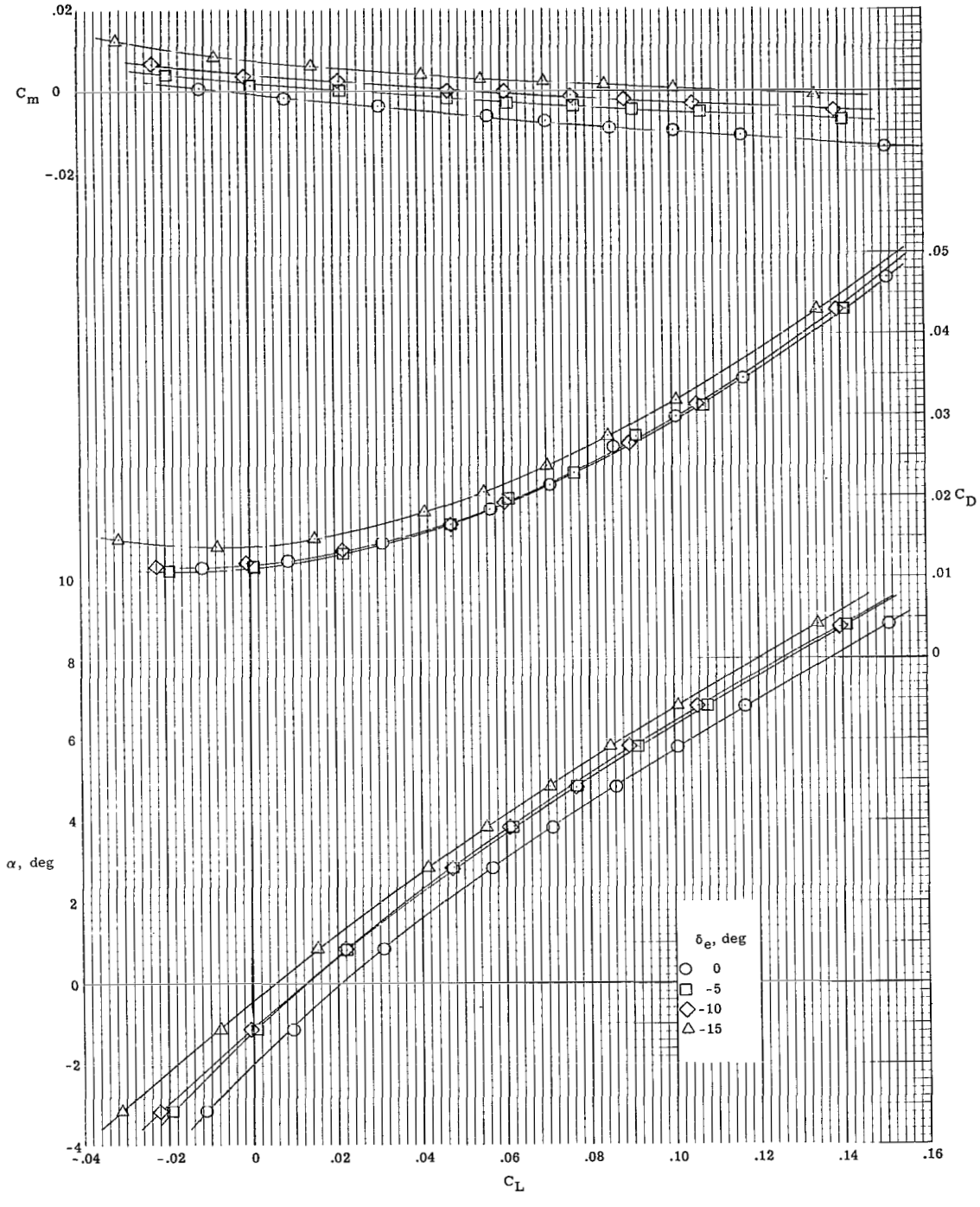

(c) Wing-body-tail-nacelle. $R_l = 6 \times 10^6$.

Figure 8.- Concluded.

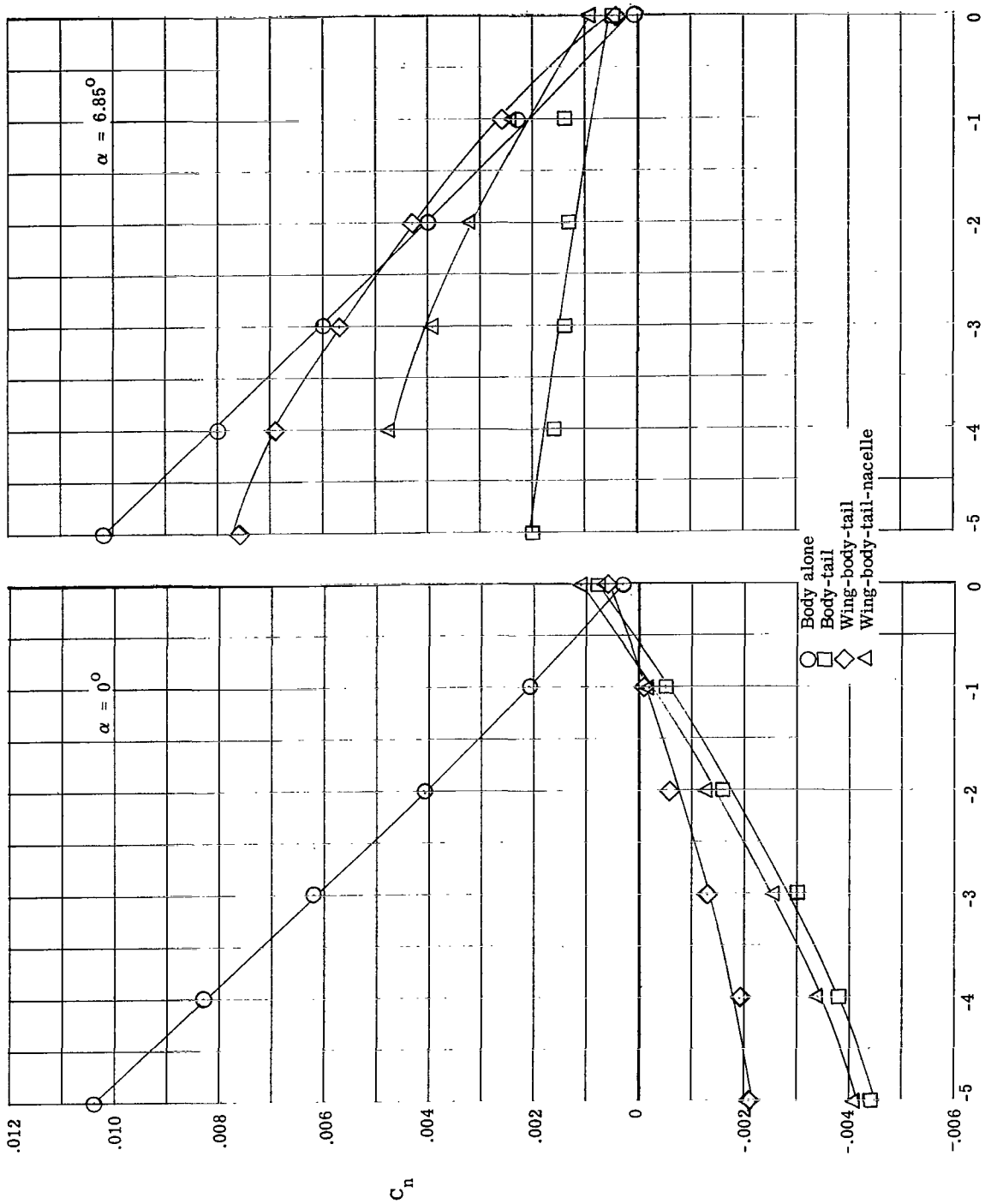

Figure 9.- Component breakdown in sideslip. $R_l = 6 \times 10^6$.

NASA-Langley, 1970 — 1 L-6803

NATIONAL AERONAUTICS AND SPACE ADMINISTRATION
WASHINGTON, D. C. 20546
OFFICIAL BUSINESS

FIRST CLASS MAIL

POSTAGE AND FEES PAID
NATIONAL AERONAUTICS AND
SPACE ADMINISTRATION

"The aeronautical and space activities of the United States shall be conducted so as to contribute . . . to the expansion of human knowledge of phenomena in the atmosphere and space. The Administration shall provide for the widest practicable and appropriate dissemination of information concerning its activities and the results thereof."

—NATIONAL AERONAUTICS AND SPACE ACT OF 1958

NASA SCIENTIFIC AND TECHNICAL PUBLICATIONS

TECHNICAL REPORTS: Scientific and technical information considered important, complete, and a lasting contribution to existing knowledge.

TECHNICAL NOTES: Information less broad in scope but nevertheless of importance as a contribution to existing knowledge.

TECHNICAL MEMORANDUMS: Information receiving limited distribution because of preliminary data, security classification, or other reasons.

CONTRACTOR REPORTS: Scientific and technical information generated under a NASA contract or grant and considered an important contribution to existing knowledge.

TECHNICAL TRANSLATIONS: Information published in a foreign language considered to merit NASA distribution in English.

SPECIAL PUBLICATIONS: Information derived from or of value to NASA activities. Publications include conference proceedings, monographs, data compilations, handbooks, sourcebooks, and special bibliographies.

TECHNOLOGY UTILIZATION PUBLICATIONS: Information on technology used by NASA that may be of particular interest in commercial and other non-aerospace applications. Publications include Tech Briefs, Technology Utilization Reports and Notes, and Technology Surveys.

Details on the availability of these publications may be obtained from:

SCIENTIFIC AND TECHNICAL INFORMATION DIVISION

NATIONAL AERONAUTICS AND SPACE ADMINISTRATION

Washington, D.C. 20546